



Models of coral growth: spontaneous branching, compactification and the Laplacian growth assumption[☆]

Roeland Merks*, Alfons Hoekstra, Jaap Kaandorp, Peter Sloot

Section Computational Science, Faculty of Science, University of Amsterdam, Kruislaan 403, 1098 SJ Amsterdam, The Netherlands

Received 25 February 2002; received in revised form 5 March 2003; accepted 13 March 2003

Abstract

In stony corals it is often observed that specimens collected from a sheltered growth site have more open and more thinly branched growth forms than specimens of the same species from more exposed growth sites, where stronger water currents are found. This observation was explained using an abiotic computational model inspired by coral growth, in which the growth velocity depended locally on the absorption of a resource dispersed by advection and diffusion (Kaandorp and Sloot, *J. Theor. Biol.* 209 (2001) 257). In that model a morphological range was found; as the Péclet-number (indicating the relative importance of advective and diffusive nutrient transport) was increased, more compact and spherical growth forms were found. Two unsatisfactory items have remained in this model, which we address in the present paper. First, an explicit curvature rule was responsible for branching. In this work we show that the curvature rule is not needed: the model exhibits spontaneous branching, provided that the resource field is computed with enough precision. Second, previously no explanation was given for the morphological range found in the simulations. Here we show that such an explanation is given by the conditions under which spontaneous branching occurs in our model, in which the compactness of the growth forms depends on the ratio of the rates of growth and nutrient transport. We did not find an effect of flow. This suggests that the computational evidence that hydrodynamics influences the compactness of corals in *laminar* flows may not be conclusive. The applicability of the Laplacian growth paradigm to understand coral growth is discussed. © 2003 Elsevier Ltd. All rights reserved.

Keywords: Morphogenesis; Coral growth; Morphologic plasticity; Phenotypic plasticity

1. Introduction

Most stony corals are colonial organisms consisting of tightly interconnected individuals, the polyps, which collectively build an external skeleton of aragonite, a form of calcium carbonate. Polyps build skeletal structures called calices, within which they reside. Calices are bound by cylindrical or polygonal walls. In some coral families, adjacent polyps share common walls, while in other families the walls are separated by skeleton deposited by a thin layer of tissue that connects

the adjacent polyps. A series of radial structures, the septa, penetrates into the calix and rises above the level of the wall. In corals whose calices do not share walls, the septa continue on the outside of the wall and link with septa from adjacent calices. Skeletal extension is achieved by outward growth of the septa and walls. In this paper, we exclusively consider stony corals whose uniformly shaped polyps form a layer of tissue that penetrates the outer surface of the coral skeleton. Thus, we do not consider corals from the *Acroporidae* family in which the tissue completely permeates the skeleton, where there are no dissepiments and where distinct axial and radial polyps are found. As the coral grows, the lower surface of the tissue is periodically lifted within the skeleton and unoccupied skeletal regions are cut off by deposition of thin bulkheads parallel to the coral surface, called dissepiments (Wells, 1969; Barnes and Lough, 1992; Vermeij et al., 2001). The dissepiments are supported between the outwardly growing skeletal structures. Polyps have a maximum diameter that is

[☆] Colour images, movies and three-dimensional images of the simulation results shown in this article have been made available as on-line supplementary material.

*Corresponding author. Tel.: +31-20-5257582; fax: +31-20-5257490.

E-mail addresses: post@roelandmerks.nl (R. Merks), alfons@science.uva.nl (A. Hoekstra), jaapk@science.uva.nl (J. Kaandorp), sloot@science.uva.nl (P. Sloot).

URL: <http://www.science.uva.nl/research/scs/>.

characteristic of the species. Once they reach this maximum diameter they divide, which is achieved by the formation of a wall that divides the calix, and the surrounding skeleton in corals which do not share walls, into two. Tissue growth and skeletal growth are tightly linked because the tissue is supported by skeleton and the skeleton is deposited by tissue. Tissue growth and skeletal growth are, however, not necessarily controlled or limited by the same factors, and variation in their relative rates of growth is thought to be an important source of morphological variation (Barnes, 1973; Barnes and Lough, 1992; Darke and Barnes, 1993).

The coral growth process generates a wide range of colony morphologies; examples are spherical, plate-like and branching growth forms. These morphologies are species specific, but also show high intraspecific variability. This intraspecific variability is probably caused by environmental parameters, such as light availability and the amount of water flow. The effect of light availability was studied in two pioneering coral modelling studies (Graus and Macintyre, 1976; Graus and Macintyre, 1982), and the effect of fluid flow on coral growth was studied in previous work by Kaandorp et al. (Kaandorp et al., 1996; Kaandorp and Sloot, 2001; Kaandorp, 2001). In the present paper we focus on two issues regarding that work. First, we study abiotic mechanisms of branching growth, and discuss whether such mechanisms can occur in corals. Thereafter we reinvestigate the model study of Kaandorp and Sloot (2001) where it was suggested that growth forms generated in a simple surface deposition model become more compact as advective transport of resources becomes more important.

One of the main questions in the study of the morphogenesis of branching corals is the branching mechanism. The branching pattern of many stony corals is probably tightly genetically regulated, since branches in many corals are added according to typical, species specific architectural rules (Dauget, 1991). In *Stylophora pistillata*, for example, such architectural rules generate a nearly spherical colony shape, that regenerates when damaged (Loya, 1976; Rinkevich, 2001, 2002). This regulation of the growth form is often thought to be mediated by chemical signals excreted into the water, the *isomones* (Rinkevich and Loya, 1985). Branching patterns also often arise in abiotic growth processes, such as viscous fingering, electric discharge and crystallisation. The development of such patterns is explained with models of diffusion-limited aggregation (DLA) (Witten Jr. and Sander, 1981) and Laplacian growth (see for example Mineev-Weinstein and Dawson, 1994; Magdaleno and Casademunt, 1998 and references therein). In such models, the growth of the pattern depends locally on the value of an external field that may either describe the concentration of aggregating particles, as in the case of DLA, or a pressure or electric

field, as in the case of viscous fingering or electric discharge. The branching patterns that arise from such abiotic growth processes are often similar in appearance to the patterns that arise in biotic growth processes, such as coral growth. This similarity suggests the possibility that in these biotic growth processes a comparable Laplacian growth mechanism may be at work.

Abiotic growth models inspired by coral growth may help in understanding for which aspects of coral morphogenesis abiotic processes may provide *sufficient* explanation (this does *not* imply that these mechanisms provide *all* the explanation), and for which aspects genetic regulation is necessarily responsible. In these models the basic assumption is that the growth rate directly depends on the local availability of organic or inorganic resources. Evidence for this so-called *resource-dependent growth* is indirect. The availability of dissolved inorganic carbon has been shown to limit the rate of photosynthesis in *Pocillopora damicornis* (Lesser et al., 1994), which is a limiting factor for calcification (Barnes and Chalker, 1990; Gattuso et al., 1999). The calcification rate of a coral community was found to depend linearly on the saturation state of calcium carbonate (Langdon et al., 2000). Organic nutrients, such as zooplankton and fine particulate matter are crucial for coral growth (see Sebens et al., 1997; Anthony, 1999 and references therein).

Two models of resource-dependent growth have been proposed by Kaandorp et al. In their *aggregation* model (Kaandorp et al., 1996; Kaandorp, 2001) coral growth was modelled as an advection–diffusion limited Meakin growth process (Meakin, 1986), which is closely related to diffusion-limited aggregation (Witten Jr. and Sander, 1981). A model that is more similar to Laplacian growth is the hydrodynamically influenced radiate accretive growth model (HIRAG model) (Kaandorp and Sloot, 2001; Kaandorp, 2001), in which the growth of the simulated coral proceeds by the iterative accretion of growth layers whose thickness is dependent on the local flux over the coral surface of a resource transported by advection and diffusion. Using that model, the observation that corals growing at exposed growth sites have more compact growth forms than corals growing at sheltered growth sites (see for example Kaandorp, 1999) was assessed. When resource transport was primarily driven by diffusion, thinly branched growth forms developed in the model. As the diffusion coefficient was lowered and advective transport became relatively more important, more compact growth forms developed in the HIRAG model.

In this paper we address two previously unresolved issues regarding the HIRAG model. Firstly, the splitting of branches was previously driven by a heuristic curvature rule, that *enforced* the branches to split as soon as a pre-set minimum curvature was reached. This curvature rule estimated “the amount of contact with

the environment [...] by measuring the local radius of curvature [...] on the triangulated surface of the object” (Kaandorp and Sloot, 2001). In the same work it was shown that growth forms developing without the curvature rule did not branch spontaneously. For this reason only the regulation of the overall branching pattern by the nutrient field, and not the mechanism of branch splitting could be assessed. From the Laplacian growth literature, however, it is known that branch splitting can occur spontaneously under the influence of a branching instability (see for example Mineev-Weinstein and Dawson, 1994; Magdaleno and Casademunt, 1998 and references therein). Since the HIRAG model without the curvature rule is structurally similar to a three-dimensional Laplacian growth model, we expected that such spontaneous branch splitting can also occur in the HIRAG model, which we investigate in this paper. Secondly, in this paper we address the mechanism behind flow-induced compactification. In agreement with observations on real corals (such as Kaandorp, 1999), in the original HIRAG model more compact growth forms developed when advective transport became relatively more important. However, the mechanism behind this phenomenon was not understood. We aim to explain it in the present paper.

The remainder of this article is organised as follows. In Section 2 we introduce the hydrodynamically influenced radiate accretive growth (HIRAG) model, of which several aspects have been improved relative to the original model (Kaandorp and Sloot, 2001). In Section 3.1 we present the appearance of spontaneous branch splitting in the HIRAG model and discuss under which conditions it appears. Using this observation, we explain in Section 3.2 why in the original model more compact growth forms are found as the influence of advective transport becomes more important. Finally, in Section 4 we discuss the relevance of these results for understanding the mechanism of branching coral growth.

2. Methods

The present work is based on the advection–diffusion limited accretive growth model by Kaandorp et al. (Kaandorp, 1995; Kaandorp and Sloot, 2001). In this model, coral growth is modelled using as a resource-dependent accretive growth process (Kaandorp, 1994), where the dispersion of resource in the surrounding water is modelled by numerically solving the equations of fluid flow and the advection–diffusion equation. The outer boundary of the coral tissue is represented by a curved surface. The periodic retreat of the tissue from the skeleton, after which a dissepiment is left behind, is modelled by constructing a new outer surface over and parallel to the previous one. The local extension of

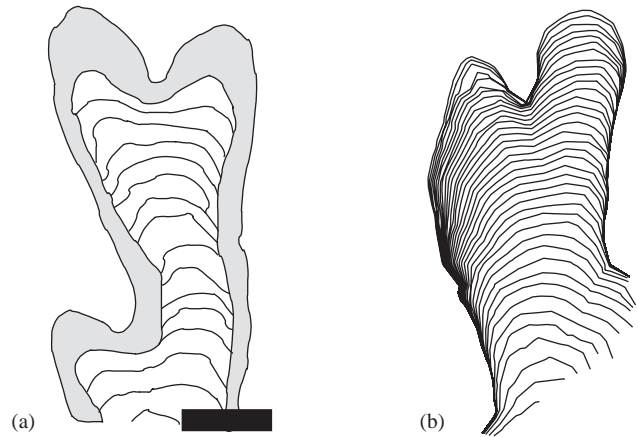


Fig. 1. Modelling accretive growth. (a) Redrawn after Fig. 9(d) of (Le Tissier et al. (1994)). The position of dissepiments in a cross-section of *Porites porites*. The grey area was formerly occupied by tissue. Scale bar = 1 cm. (b) Cross-section of a branch of a simulated object, the lines indicate the successive surfaces.

skeleton is determined by a *growth function*, which is dependent on the availability of a resource dispersed by the surrounding simulated fluid. This process generates a growth form whose inner structure resembles the pattern formed by the dissepiments in real corals. This is exemplified in Fig. 1, where a cross-section of a branch of a simulated coral (Fig. 1b) is compared to the position of the dissepiments in a skeletal slice of *Porites porites* (Fig. 1a, redrawn after Le Tissier et al., 1994).

More formally, the growth model is described as follows. The coral surface is conceptually modelled as a curved, continuous surface that is approximated by a triangular mesh. The mesh consists of vertices v_i and intervertex links \vec{A}_{ij} (Fig. 3). Each vertex v_i consists of a coordinate x_i, y_i, z_i and of a vector of locally measured growth parameters $\vec{\mu}_i$, as described later in this section. The advective and diffusive transport of resources is modelled on a cubic lattice using numerical simulations of the Navier–Stokes and advection–diffusion equations. The simulation proceeds as follows (see Fig. 2). The initial geometry is a triangulised hemisphere, that contains 81 vertices (Fig. 2a). The hemisphere is mapped onto the cubic lattice, for which we use a triangle voxelisation method (Huang et al., 1998), after which the resulting hollow shell is filled using a fast, heuristic three-dimensional seed fill algorithm (Fig. 2b). The fluid flow around the voxelised geometry can then be calculated (Fig. 2c) by numerically solving the Navier–Stokes equations of (incompressible) fluid flow,

$$\begin{aligned} \vec{\nabla} \cdot \vec{u} &= 0, \\ \frac{\partial \vec{u}}{\partial t} &= -(\vec{u} \cdot \vec{\nabla}) \vec{u} - \vec{\nabla} P + \nu \vec{\nabla}^2 \vec{u}, \end{aligned} \quad (1)$$

where \vec{u} is the velocity, t is the time, P is the pressure and ν is the kinematic viscosity. We do not solve the Navier–Stokes equations directly; instead we use the lattice

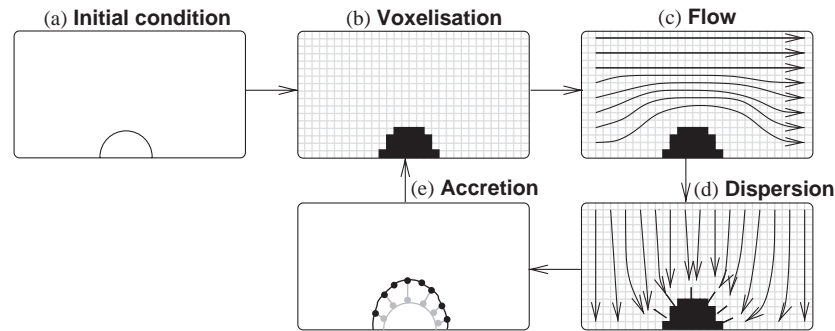


Fig. 2. Schematic flowchart of the simulation. The initial sphere, represented by a triangular mesh containing 162 vertices, is voxelised in a cubic lattice (b), after which the fluid flow (c) and resource dispersion (d) are calculated until stability. The resource flux ϕ_i is measured using a “probe” (shown as a black line in d) at each vertex of the coral surface. In the accretion step (e), a new triangular mesh is built on top of the previous mesh, where the growth rate depends on a function g of the resource flux. This mesh is voxelised (b), initiating a new growth cycle.

Boltzmann–Bhatnagar–Gross–Krook method (Succi, 2001).¹ The flow is driven by imposing a constant velocity at the top plane. The ground plane and the coral are treated as solids with a no-slip boundary condition, i.e. the fluid velocity is zero, whereas the lateral boundaries are periodic. In this paper we only consider stable flow fields (i.e. laminar and time-independent). In the simulations of Section 3.1 the flow field is iteratively solved until the change per unit time of the mean velocity $\langle |\vec{u}| \rangle$ falls below a convergence threshold,

$$\left| \frac{\Delta \langle |\vec{u}| \rangle}{\Delta t} \right| < \theta_{NS}, \quad (2)$$

with θ_{NS} some small number. As soon as the flow has stabilised according to Eq. (2), the transport of the resource R by advection and diffusion and the uptake of resources by the growing coral colony is simulated by numerically solving the advection–diffusion equation (Fig. 2d),

$$\frac{\partial R}{\partial t} + \vec{u} \cdot \vec{\nabla} R = D \vec{\nabla}^2 R, \quad (3)$$

where R is the resource concentration and D is the diffusion coefficient and the velocity \vec{u} is taken from the stabilised flow field. The top plane is kept at a fixed concentration $R = 1.0$. At the side planes we have applied a periodic boundary condition, whereas the ground plane and the coral surface are kept at a concentration of $R = 0$, hence assuming that the coral tissue actively takes up resources and that resources reaching the sea floor are taken up by competing sessile organisms such as hydrozoans, coralline algae and other corals. These boundary conditions generate concentration gradients over the simulation box. Indeed, such concentration gradients of zooplankton occur at night in coral reefs of the Red Sea, with high concentrations of plankton near the sea surface and much lower concentrations close to the sea floor (R. Horzman and

A. Genin, unpublished data). The advection–diffusion equation is solved using the moment propagation method (see Merks et al., 2002 and references therein). In most simulations (except for those in Section 3.2) the advection–diffusion equation is iteratively solved until the change per unit time of the total resource mass falls below a convergence threshold,

$$\left| \frac{\Delta(\sum_x R)}{\Delta t \sum_x R} \right| < \theta_{AD}. \quad (4)$$

The relative importance of advective vs. diffusive transport processes is expressed by the dimensionless Péclet number,

$$Pé = \frac{\langle |\vec{u}| \rangle L}{D}, \quad (5)$$

where $Pé$ is the Péclet number, $\langle |\vec{u}| \rangle$ is the mean flow velocity and L is a characteristic length. Throughout this paper we are exclusively using the *lattice Péclet number* $Pé_{lat}$ with the characteristic length set to $L = 1$ lattice unit (l.u.), the distance between two neighbouring nodes in the computational grid.

As soon as the resource influx at the top plane balances the absorption of resources by the ground plane and the coral, we measure the resource flux ϕ_i at each vertex of the mesh by probing the resource concentration R_i at a distance $l = 3$ l.u. from the vertex v_i along the surface normal (the probes are shown as black lines in Fig. 2d). Since $R = 0$ at the coral surface, the resource gradient ∇R at the surface can be approximated as R/l . According to Fick’s law, the flux per unit area $\phi_i = D \nabla R = DR/l$. As the object grows towards the top plane, the resource fluxes ϕ_i increase. In order to fix the growth rate, the resource absorption is normalised against the maximum resource flux, $\phi_i \mapsto \phi_i / \phi_{max}$. Note that the normalised fluxes are independent of D/l , so we can simply set $\phi_i = R_i / R_{max}$. Using this flux normalisation we fix the thickness of the boundary layer between the growing coral colony and the rest of the sea water, in which the

¹We used a kinematic viscosity of $\nu = \frac{1}{6}$ in lattice units.

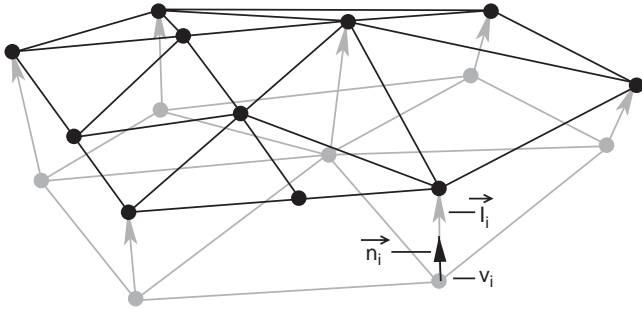


Fig. 3. Diagram of an accretive growth step. Vertical extension of the skeleton is simulated by building an element \vec{l}_i (shown as grey arrows) on top of the vertices (grey disks), in the direction of the local surface normal vector \vec{n}_i . The length of the element \vec{l}_i depends on the local measurements $\vec{\mu}_i$ and on the growth function g . After the construction of a new layer, it is refined by inserting and removing vertices. This procedure of mesh refinement is explained in Appendix B. The new, refined layer is shown in black.

nutrient concentration is assumed constant and constantly mixed. An alternative interpretation is given in Appendix A. We have also carried out simulations without this normalisation; these results do not differ qualitatively from the ones reported in this paper (data not shown).

After the resource fluxes have been measured, we move back to the triangular mesh representation and carry out an *accretive growth* step (Fig. 2e). On top of the previous layer, a new layer of skeleton is built, whose local thickness depends on (amongst others) the resource flux ϕ_i . In each accretion step, the vertical extension of the skeleton is simulated by placing an element \vec{l}_i on top of each vertex v_i along the surface normal vector \vec{n}_i at vertex v_i , according to

$$\vec{l}_i = g(\vec{\mu}_i)\vec{n}_i, \quad (6)$$

where $g(\vec{\mu}_i)$ is a *growth function* that takes the local measurements $\vec{\mu}_i$ (in the present case the local nutrient flux) and returns a (scalar) growth velocity. We do not explicitly model the secondary thickening of the skeleton. We have used several growth functions for the experiments carried out in this paper that we describe in Section 3. The vertex v_i is moved to the end of the element \vec{l}_i , as if the coral surface is pushed upwards by excreting calcium skeleton. In this process, the value of $\vec{\mu}_i$ is retained. As a result of this accretion, the surface locally expands or contracts, depending on the local surface curvature. To make sure that the vertices remain equally distributed over the surface, vertices are inserted or removed. In this way skeletal accretion remains possible over the whole surface. A description of the methods used for the insertion and removal of vertices is given in Appendix B.

A simple measure of compactness was used to characterise the morphologies. We define the *compactness* C of the coral as the fraction of solid material inside

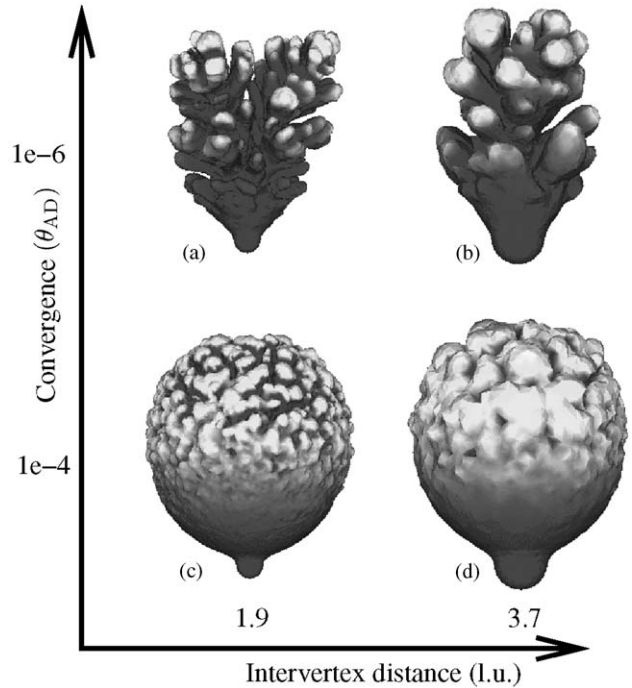


Fig. 4. Results of the resource flux-driven HIRAG model (growth function 8) for increasing resource field convergence (vertical axis) and increasing intervertex distance (horizontal axis); 83 accretive growth cycles; computational grid has size 200^3 ; No flow ($\langle \vec{u} \rangle = 0$, $Pe = 0$); (a) $C = 0.39$; (b) $C = 0.55$; (c) $C = 0.89$; (d) $C = 0.91$. Movies of the developmental sequences, colour images and three-dimensional images are part of the on-line supplementary material.

the convex hull² of the object,

$$C \equiv \frac{V_{object}}{V_{hull}}, \quad (7)$$

where V_{object} is the volume of the object, and V_{hull} is the volume of the convex hull. The convex hull was determined using the quickhull algorithm (Barber et al., 1996). Our definition of compactness is dimensionless, making it size invariant and exclusively dependent on the morphology. It would be easily measured in the field, by dividing the displaced volume of the coral by the displaced volume of the same coral wrapped in plastic.

The objects have been visualised using the General Mesh Viewer (GMV).³ Colour images, three-dimensional images in VRML format and movies of the developmental sequences have been made available online⁴. The simulations were carried out on a Linux Beowulf cluster of 58 AMD Athlon processors running at 700 MHz, with 256 or 512 MByte internal memory per processor. The accretive growth algorithm was executed on a single processor, while the numerical

²Think of the convex hull as the space enclosed by the tightest possible gift wrapping around the object.

³GMV can be obtained from <http://www-xdiv.lanl.gov/XCM/gmv/>.

⁴<http://www.science.uva.nl/~roel/JTB/>.

methods for the Navier–Stokes [Eq. (1)] and advection–diffusion [Eq. (3)] equations have been parallelised (Kandhai et al., 1998). The simulations of the HIRAG model without curvature rule in Section 3.1 were carried out on 16 processors. The flow and advection–diffusion calculations were the main bottleneck. The computer time needed for the objects shown in Fig. 4 was 1:30 hours for $\theta_{AD} = 10^{-4}$ and 9 days for $\theta_{AD} = 10^{-6}$. Note that in these simulations no flow field was calculated. The calculation of each of the objects shown in Fig. 6 took 40 days of computer time on 16 processors. A major fraction of this time was used for the flow calculations. The simulations of the model of Section 3.2 were considerably less demanding, for which reason we needed only 6 to 12 processors per simulation. These took on the order of 3 up to 12 h each, depending on the amount of processors used for the flow and advection–diffusion calculations, and on the amount of triangles needed to describe the accretive growth layers.

3. Results

3.1. Spontaneous branch splitting

In the original HIRAG model (Kaandorp and Sloot, 2001) it was not possible to assess the mechanism of branch splitting in coral growth, since a *curvature rule* enforced the branches to split. Without this heuristic, no branch splitting occurred and so-called “lobed” growth forms developed, that have a folded surface and no second order branches. In this section we show that spontaneous branch splitting *does* occur in the HIRAG model. We have used the original formulation of the curvature-independent HIRAG model (Kaandorp and Sloot, 2001). Aiming to keep the model as simple as

possible, the growth is exclusively driven by the local resource flux as in the linear growth function,

$$g(\vec{\mu}) = s\mu_1, \quad (8)$$

where $\mu_1 = \phi_i/\phi_{max}$. ϕ_i is the resource flux at vertex v_i and ϕ_{max} is the maximum resource flux occurring during the growth cycle. s is the thickness of a growth layer and is set to 1.25 l.u. for the simulations in this section. This setting ensures that in the computational grid the object grows by steps of at most one solid node thick. This growth function is nearly identical to the growth function in which “only the influence of the local availability of simulated nutrient is included” (Kaandorp and Sloot, 2001), except for the omission of a minimal growth velocity threshold tr . The dynamic stopping criteria [Eqs. (2) and (4)] are used and a computational grid of 200^3 is used.

In Fig. 4 we show four realisations of the HIRAG model with the growth function given by Eq. (8) in the diffusion-limited regime (that is, $\langle |\vec{u}| \rangle = 0$) for strict and loose resource convergence thresholds θ_{AD} . For loose convergence thresholds ($\theta_{AD} = 10^{-4}$) we found very compact, nearly spherical non-branching objects (Fig. 4c), agreeing to the results obtained by Kaandorp and Sloot (2001). However, for strict convergences ($\theta_{AD} = 10^{-6}$) we found branched, open structures (Fig. 4a). Thus spontaneous branch splitting *does* occur in the HIRAG model, provided that the resource field has converged well enough. The initial condition also has an effect on the growth form. An initial sphere of radius $r = 8$ l.u. and $r = 16$ l.u. was used for the objects in the left and right column, respectively. The initial radius determines the initial mean link length $|\langle \vec{A}_{ij} \rangle|_{init}$, which dictates the spacing of the vertices over the coral surface (see Section 2).

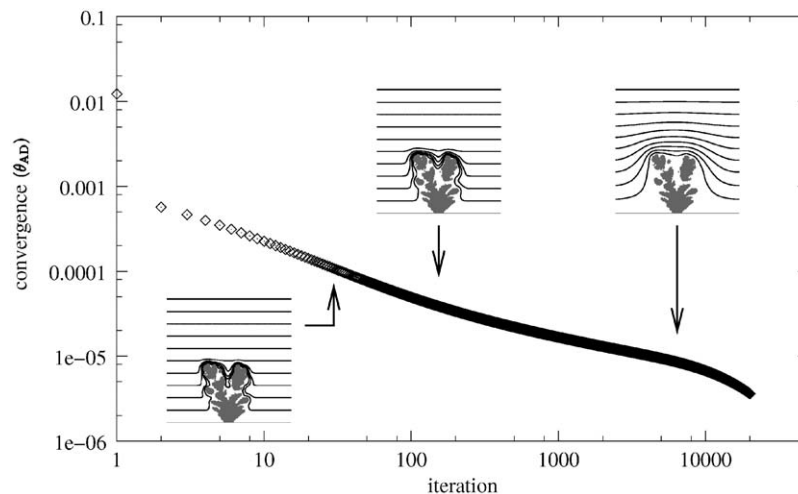


Fig. 5. Convergence of the resource field as a function of the iteration number, starting from a linear initial resource field. Insets: resource fields on an xz -section ($y = 100$ l.u.) of the upper left object of Fig. 4 for a convergence of $\theta_{AD} = 10^{-4}$ (left), $\theta_{AD} = 5 \times 10^{-5}$ (middle) and $\theta_{AD} = 10^{-5}$. Isolines indicate concentrations of $R = 0.1$ (bottom) to $R = 1.0$ (top) with increments of 0.1.

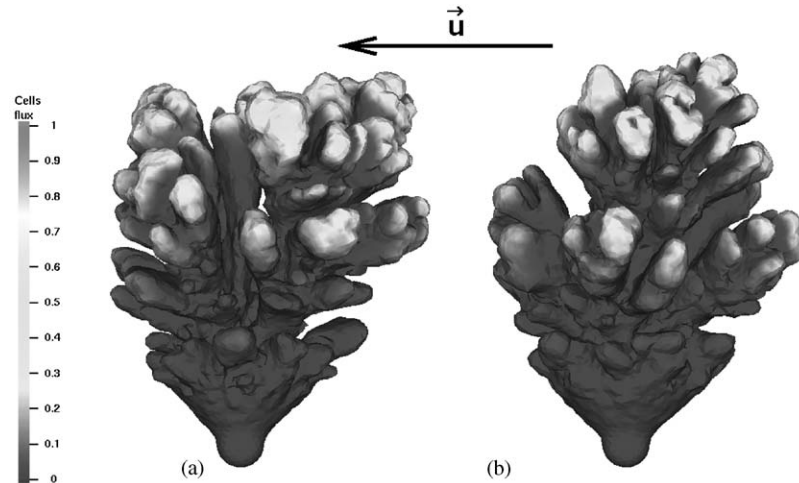


Fig. 6. Branching objects grown with the resource flux-driven HIRAG model (growth function given by 8) in a mono-directional flow directed from right to left. Intervertex distance was 1.9 (compare Figs. 4a and b). (a) 84 growth cycles, $\bar{u}_{max} = 0.04$, $D = 0.17$, $\bar{P}e_{lat} = 0.24$, $C = 0.39$; (b) 84 growth cycles, $\bar{u}_{max} = 0.04$, $D = 0.07$, $\bar{P}e_{lat} = 0.60$, $C = 0.43$. Movies of the developmental sequences, colour images and three-dimensional images are part of the on-line supplementary material.

In Fig. 5 we have studied the convergence of the resource field of the object of Fig. 4a by measuring the relative change in the resource field as defined in Eq. (4). Slices of the resource field at a convergence of $\theta_{AD} = 10^{-4}$, 5×10^{-5} and 5×10^{-5} are shown as well. For this figure the convergence was started from a linear resource field. Note that in the growth simulations we start with the last resource field of the previous growth cycle. The field converges progressively more slowly as the solution approaches stability. After about 10^4 iterations we observe a slight speed-up of the resource field convergence. We have not investigated this effect. Only after the strict convergence criterion of $\theta_{AD} = 5 \times 10^{-5}$ is met, a depletion zone with very small resource concentrations has formed between the branches and around the coral. Apparently such detail in the resource field is important for spontaneous branch splitting.

Growth forms with Eq. (8) were also developed in a low velocity flow. The velocity at the top plane was set to $\bar{u}_{max} = 0.04$ l.u., where the flow was directed parallel to the top plane and the flow field was iterated until a convergence of $\theta_{NS} = 10^{-8}$ was reached. The flow field convergence typically took on the order of 100–5000 lattice Boltzmann iterations, depending on the complexity of the growing object.

In Fig. 6 two of the resulting objects are shown. In both cases a resource field convergence of $\theta_{AD} = 10^{-6}$ was used. The objects slightly bent towards the flow, but we did *not* find apparent effects of the laminar flow field on the compactness of the growth forms (Table 1). When we increased the Péclet number by using a smaller diffusion coefficient (Fig. 6, right), the growth form did not compactify. However, when we used a smaller degree of resource field convergence (i.e. $\theta_{AD} = 10^{-4}$),

Table 1

Compactness of the simulated growth forms developed with the growth function of Eq. (8)

\bar{u}	D	$\bar{P}e_{lat}$	Compactness ($n = 1$)	Fig.
0.0	0.167	0	0.39	4a
0.0	0.167	0	0.55	4b
0.0	0.167	0	0.89	4c
0.0	0.167	0	0.91	4d
0.0	0.167	0.24	0.39	6a
0.0	0.067	0.60	0.43	6b

the growth form did compactify (data not shown) like in the diffusion-limited case of Fig. 4. Thus we did not find an apparent effect of the flow velocity on the compactness of the growth forms, suggesting that in the present model stable laminar fluid flows do not affect the growth form. The compactness remained unchanged even for Péclet-numbers at which flow effects were reported in previous studies (Kaandorp and Sloot, 2001).

3.2. Resource field convergence and compactification

In the previous section we showed that spontaneous branching only occurs when enough advection–diffusion is permitted, enabling the formation of depletion zones. These depletion zones may be important in explaining the observation that corals growing in exposed growth sites often have more compact, robust growth forms than corals growing under more sheltered environmental conditions. We would expect the branches to be more widely spaced depending on how well the depletion zones can develop. In this section, we reassess the question whether the suppression of depletion zones by hydrodynamics can explain the flow-induced morphologic

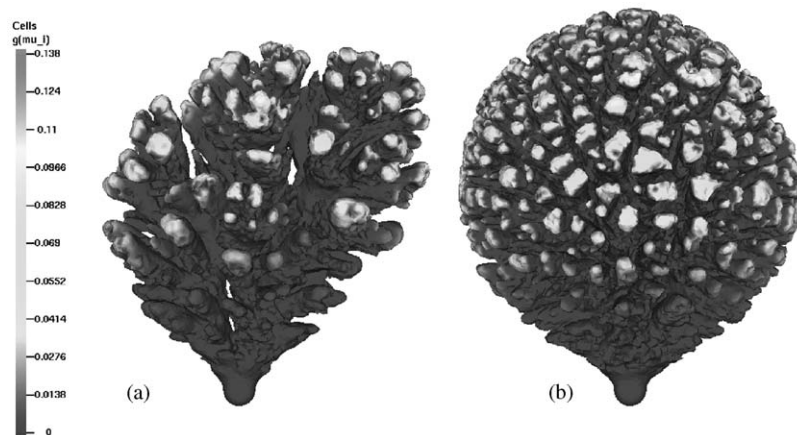


Fig. 7. Results of the diffusion-limited HIRAG-model with *curvature rule*. Eighty-five accretive growth cycles were applied in both panels. The size of the simulation box was 144^3 , the radius of the initial sphere was 8 l.u. (a) $D = 0.167$, $Pé = 0$; (b) $D = 0.017$, $Pé = 0$. Movies of the developmental sequences, colour images and three-dimensional images, and images of alternative instantiations are part of the on-line supplementary material.

compactification, as it was previously observed in the HIRAG model (Kaandorp and Sloot, 2001). In order to compare the results of the present HIRAG simulations to the previous work correctly, we reintroduced the *curvature rule* (Kaandorp and Sloot, 2001) in the growth function,

$$g(\vec{\mu}_i) = s\mu_{i,1}\mu_{i,2} \quad \forall \mu_{i,1}\mu_{i,2} > tr, \\ = 0 \quad \forall \mu_{i,1}\mu_{i,2} \leq tr, \quad (9)$$

where $tr = 0.0001$ and s is the maximum thickness of a layer, which was set to $s = \langle |\vec{A}| \rangle$, the mean length of the links in the initial condition. Following Kaandorp and Sloot (2001), the measurements $\mu_{i,1} = \phi_i/\phi_{max}$ and $\mu_{i,2} = h2_i$ contained the normalised local resource flux and an estimation of “the amount of contact with the environment”, $h2_i$. In this paper the value of $h2_i$ was calculated from the two principal curvatures κ_1 and κ_2 at vertex v_i ,

$$h2_i = \text{low_norm_curv} \times \bar{\kappa}, \quad (10)$$

where

$$\text{low_norm_curv} \\ = \Theta_1(1 - (\Theta_2(1/\kappa_2) - \text{min_curv})/ \\ \times (\text{max_curv} - \text{min_curv})) \quad (11)$$

in which $\kappa_2 < \kappa_1$ and $\bar{\kappa} = \frac{1}{2}(\kappa_1 + \kappa_2)$ is the mean curvature. The threshold function $\Theta_1(x)$ sets all negative values to 0 and all values greater than 1 to 1; $\Theta_2(x)$ sets all negative values to 0. The principal curvatures κ_1 and κ_2 were measured with the method by Meyer et al. (2002). $\text{min_curv} = 2s$ is the radius of curvature below which the growth is maximal; $\text{max_curv} = 20s$ is the radius of curvature above which the growth is set to 0. Note that, following their original definition (Kaandorp, 1994, 1995; Kaandorp and Sloot, 2001), these parameters are defined in terms of the *radius of curvature* instead of the *curvature*. Instead of using the field convergence stopping conditions as in Eqs. (2) and (4),

the simulations in this section were stopped after a fixed number of lattice Boltzmann and moment propagation iterations, thus following the simulation set-up by Kaandorp and Sloot (2001). According to that work, we used a cubic lattice of size 144^3 and 50 advection–diffusion iterations per growth cycle (Kaandorp, pers. comm.). Note that with 50 iterations a stable resource field is not reached (see Fig. 5). The radius of the initial sphere was $r = 8$ l.u.

In Fig. 7 we show two realisations of this model in a non-moving fluid. In the left panel $D = 0.167$, in the right panel $D = 0.017$. In both cases the flow velocity was $\langle |\vec{u}| \rangle = 0$, such that $Pé = 0$. For $D = 0.167$ we found relatively thinly branched growth forms (Fig. 7a.). This finding reproduces the observations in the previous work. Note that this growth form is slightly asymmetric, despite the absence of flow. When we used a smaller diffusion coefficient ($D = 0.017$), the growth forms obtained more branches and were better centred (Fig. 7b.) This finding violates the original assumption that the flow and resource fields are in equilibrium, in which case the resource field, and consequently the growth form, should be independent of the diffusion coefficient. In the original work by Kaandorp and Sloot (2001), the Péclet number was varied by exclusively changing the diffusion coefficient, while the same flow velocity was used for all simulations. For large Péclet numbers, that were obtained by lowering the diffusion coefficient keeping the flow velocity unchanged, the growth forms were found to be more compact and more spherical. Our results agree to this observation, although here we did not apply any fluid flow ($\langle |\vec{u}| \rangle = 0$, $Pé = 0$): for lower diffusion coefficients, we found more compact and more spherical growth forms. This suggests that the compactification as it was observed in the original simulations is not a Péclet-number effect; instead, the compactness appears to depend directly on the diffusion coefficient.

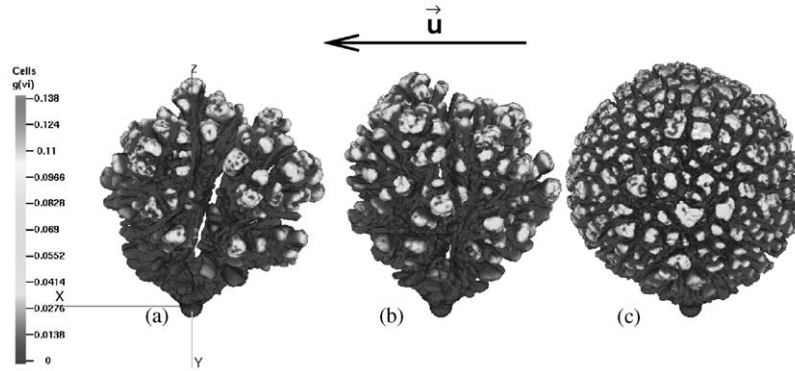


Fig. 8. Objects grown in a mono-directional flow (right to left) with the curvature rule. Viewpoint elevation is 30° relative to x -axis. The size of the LBGK-lattice is 144^3 , the size of the initial sphere is 8 l.u. (a) $\overline{P\dot{e}}_{lat} = 0.3$, $u = 0.05$, $D = 0.167$; (b) $\overline{P\dot{e}}_{lat} = 0.75$, $u = 0.05$, $D = 0.067$; (c) $\overline{P\dot{e}}_{lat} = 0.75$, $u = 0.0125$. Movies of the developmental sequences, colour images and three-dimensional images, and images of alternative instantiations are part of the on-line supplementary material.

Table 2

Compactness of the simulated growth forms developed with the growth function of Eq. (9)

\bar{u}	D	$\overline{P\dot{e}}_{lat}$	Compactness ($n = 5$)	Fig.
0.0	0.167	0	0.290 ± 0.008	7a
0.0	0.017	0	0.416 ± 0.002	7b
0.050	0.167	0.3	0.288 ± 0.003	8a
0.050	0.067	0.75	0.325 ± 0.003	8b
0.012	0.017	0.75	0.418 ± 0.004	8c

This conclusion is further supported by the results shown in Fig. 8. Objects a and b were grown in a mono-directional flow (right to left) with $\langle |\bar{u}| \rangle = 0.05$ l.u. The velocity at the top plane was set to $\bar{u}_{max} = 0.1$ l.u., a velocity that is close to the upper limits of applicability of the used lattice Boltzmann method, and similar to the velocities that were used in Kaandorp and Sloot (2001). Following that work, we applied 10 iterations of the lattice Boltzmann method per growth cycle (Kaandorp, pers. comm.), which—given the 100 to 5000 iterations per growth cycle that were needed to obtain a convergence of $\theta_{NS} = 10^{-8}$ in Section 3.1—is not sufficient to obtain a stable flow field. The diffusion coefficient for object a was $D = 0.167$, for which $\overline{P\dot{e}}_{lat} = 0.3$. The slight asymmetry in these objects is directed against the fluid flow. The compactness is not different from Fig. 7a (see Table 2), where no flow was applied. Thus, in this experiment we observed no effect of the laminar flow on the compactness. Like in Fig. 7, a smaller diffusion coefficient led to compactification and stronger branching (Fig. 8b). In this simulation $\bar{u} = 0.05$ and $D = 0.067$ which is the minimum diffusion coefficient for which the advection–diffusion method gives correct results for the used flow velocity (Merks et al., 2002), for which $\overline{P\dot{e}}_{lat} = 0.75$. When the diffusion coefficient was further lowered to $D = 0.017$ keeping the Péclet number constant by using a smaller flow velocity ($\bar{u} = 0.0125$), we found even more compact

growth forms. (Fig. 8c). Statistical testing revealed that the compactness measurements (Table 2) were not significantly different from the values of Fig. 7b, where the same diffusion coefficient was used in a still-standing fluid. The compactness of these objects is thus directly dependent on the diffusion coefficient, and not on the Péclet number.

4. Discussion

We have studied the hydrodynamically influenced radiate accretive growth model (HIRAG model) (Kaandorp and Sloot, 2001). The HIRAG model is an abiotic growth model that is inspired by coral growth. Rather than to model the morphogenesis of a specific coral species, the aim of such a model is to understand for which aspects of coral growth abiotic mechanisms provide sufficient explanation, and for which aspects biotic effects, such as genetic regulation and differential tissue and skeletal growth, must be responsible.

In the present paper we have focused exclusively on abiotic mechanisms that are sufficient to reproduce aspects of coral growth. The model of these abiotic mechanisms was deliberately kept as simple as possible. For example, we have used a linear growth function, whereas it would biologically be more plausible to use a saturated growth function. Since we think that only through a prior thorough understanding of the simplified model the effect of such more complicated assumptions can be understood, we have refrained from including a number of important biological mechanisms. For example, we could include genetic regulation in the HIRAG model by having the coral surface excrete growth suppressing “isomones” (Rinkevich and Loya, 1985; Kaandorp, 2001), or by allowing for interpolyal communication by introducing signalling chemicals diffusing over the coral surface. Also, we have ignored the fact that many modular cnidarians transfer resources

through the gastrovascular cavity (Rinkevich and Loya, 1983; Oren et al., 1997; Gateno et al., 1998), which we could model by allowing the resources to diffuse over the coral surface. Polyps subject to high flow velocities become flattened, making it impossible for them to catch food particles (Sebens et al., 1997). Including such flow-dependent resource uptake would certainly affect the simulation results. Currently we have also ignored the fact that in real corals the rates of tissue growth and skeletal growth can be controlled by different environmental factors (Barnes, 1973; Barnes and Lough, 1992; Darke and Barnes, 1993). In the present model the rate of “tissue growth”, as given by the rate of extension of the coral surface, is directly linked to the rate of “skeletal growth”. We could model such differential tissue and skeletal growth by decoupling the rates of vertex insertion and skeletal accretion and making those processes dependent on different resources. Although these biotic factors would all affect the results of our model, we have not included them in the present model. This enables us to study for which facets of coral growth abiotic growth processes provide *sufficient* explanation. Moreover, the future one-by-one inclusion of these biotic processes may provide a clear picture of their roles in shaping the coral colony.

We addressed two issues of the HIRAG model: the mechanism of branch splitting and the mechanism of compactification under the influence of fluid flow. In Kaandorp and Sloot (2001) the splitting of branches was enforced by a *curvature* rule. Thus, in that model it was not possible to study the mechanism of branch splitting. In Section 3.1, we demonstrated that branch splitting can also occur in the HIRAG model if no *curvature* rule is used, provided that the resource field is solved until near stability. Branch splitting occurred only if the time-scales of growth and resource dispersion were well separated, that is if resource diffusion is a much faster process than skeletal growth. This assumption sets the diffusion-limited HIRAG model in the class of Laplacian growth models (like viscous fingering). Laplacian growth forms often have a few dominating branches that absorb more resources than the smaller ones, thus creating a zone of resource depletion around them. This sets off a branching instability, where the growth of smaller branches is suppressed by the larger branches. Such *stagnation points* are well known from theoretical, numerical and experimental studies of Laplacian growth (see for example Mineev-Weinstein and Dawson, 1994; Magdaleno and Casademunt, 1998 and references therein). If the depletion zones are not allowed to form well, the branching instability does not occur and the surface grows out at a uniform rate, resulting in spherical, compact growth forms.

It is well known that branching instabilities occur in Laplacian growth systems in which the growth velocity does not explicitly depend on the local curvature. For

example, it was shown numerically and theoretically that in the absence of surface tension (which is a stabilising curvature-dependent effect) tip splitting, stagnation points and other features of viscous fingering occur (Mineev-Weinstein and Dawson, 1994; Magdaleno and Casademunt, 1998). Although in the HIRAG model the curvature rule is not a necessary condition for branching (Section 3.1), we do not think that it is free of curvature effects. In the HIRAG model we observe a positive correlation between the resolution of the surface discretisation and the size of the branches (Fig. 4). The surface discretisation, which may reflect the density of polyps, appears to determine how strongly the surface can be bent. We may therefore interpret it as an implicit surface tension effect, which has the effect of smoothening out high-frequency irregularities on the surface.

The conditions under which spontaneous branching occurs, suggest the explanation for the observations in the original simulations of the curvature-dependent model (Kaandorp and Sloot, 2001), where a positive correlation was found between the object’s compactness and the Péclet number. In these simulations only the diffusion coefficient was changed to vary the Péclet number, while the flow velocity was kept unchanged in all simulations and the morphologies were not compared to the morphologies that develop in the absence of flow. We found the same trend here (Fig. 7) when we changed the diffusion coefficient in a stationary fluid ($\langle |\vec{u}| \rangle = 0$ and $Pe = 0$) with a fixed number of iterations as in the work by Kaandorp and Sloot (2001). Moreover, when we imposed a flow with a velocity near the limits of applicability of the used lattice Boltzmann method, the growth forms did not change (Fig. 8a). The growth forms compactified when we increased the Péclet number by lowering the diffusion coefficient, keeping the flow velocity at the same high level (Fig. 8b). If the diffusion coefficient was further lowered, concurrently lowering the flow velocity in order to keep the Péclet number constant, we found strong compactification (Fig. 8c).

These results do not support the conclusion that for “(...) an increasing influence of hydrodynamics, the simulated morphologies (are) gradually transformed from thin-branching ones into more spherical and compact morphologies” (Kaandorp and Sloot, 2001). The limited number of iterations in solving the resource and flow fields in their simulations was responsible for the observed dependence of the compactness on the diffusion coefficient. For the final, stable solution of the diffusion equations, the value of the diffusion coefficient is of course irrelevant. But if the advection–diffusion equations are solved numerically for a fixed, small number of iterations this stable solution is not reached. In fact, for smaller diffusion coefficients the solution remains even further from stability, because the time to reach the stable solution becomes longer. In such a case

sufficient depletion zones around the branches may not form, which results in more compact growth forms and more branches as in Figs. 7b and 8c. With the dynamic stopping criterion that was used in Section 3.1, the deviation from the stable solution does no longer depend on the diffusion coefficient, but only on the stopping criterion. Indeed, there the compactness depended on the stopping criterion and not on the diffusion coefficient (Figs. 4 and 6). The original assumption of the HIRAG model is that resource transport is a much faster process than coral growth. The results presented here suggest strongly that the fact that these time-scales were not well separated in the original simulations, resulted in an incorrect interpretation of the compactification effect.

We investigated whether natural coral growth may be considered a Laplacian growth process by considering the real time-scales of growth and transport. These are compared by estimating the time needed to diffuse over the yearly skeletal extension rate (i.e. the growth caused by extension of vertical skeletal elements, ignoring secondary thickening). Assuming a transport mechanism that can be approximated by diffusion, the time needed to transport a resource over a distance Δx is estimated as

$$t_D \approx \frac{(\Delta x)^2}{D}. \quad (12)$$

The skeletal extension rate varies between coral species and on environmental parameters such as the sea surface temperature (Lough and Barnes, 2000). A short overview of skeletal extension rates reported in the literature is given in Table 3, from which we derive a typical yearly extension rate for branching corals of 17 mm year⁻¹. The value for *Acropora* was not included in this estimate, since this genus is not covered by the HIRAG model.

The typical diameter of particles captured by colonies of *Madracis mirabilis* is about 1 mm (Kaandorp and Sloot, 2001). A typical passive diffusion coefficient in water of such particles is $5 \times 10^{-16} \text{ m}^2 \text{ s}^{-1}$ (Weast et al., 2000). Using Eq. (12) we have estimated that the time needed for a fair amount of these particles to diffuse 17 mm is about 18000 years. Hence it is not correct to approximate coral growth with a Laplacian growth process based on such passive particle diffusion alone. The diffusion coefficients of food particles increase substantially by assuming additional mechanisms. Many organic food particles display active, random movement. For example, a guess of the diffusion coefficient of the unicellular alga *Chlamydomonas nivalis*, based on mean free path calculations, ranges from 5.0×10^{-9} to $5.0 \times 10^{-7} \text{ m}^2 \text{ s}^{-1}$ (Kessler, 1986), for which the diffusion times are in the order of 8 h to 5 min. Kaandorp and Sloot (2001) estimated the diffusion coefficient of actively moving food particles of about 1 mm in

Table 3
Brief overview of skeletal extension rates as reported in review papers

Species	Growth form	Extension rate (mm year ⁻¹)
<i>Porites</i> spp.	Massive	12.0 ± 4.9 ^a
<i>Porites</i> spp.	Branching and columnar	2 to 48 (10) ^b
<i>Pocillopora damicornis</i>	Branching	9 to 57 (28) ^b
<i>Acropora</i> spp.	Branching	21 to 172 (77) ^b
<i>Montastrea annularis</i>	Massive	5 to 25 (11) ^c
<i>Pocillopora damicornis</i>	Branching	1.6 to 35.9 (19) ^c

^a Lough and Barnes (1997).

^b Harriott (1999).

^c Buddemeier and Kinzie III (1976).

diameter at $3.5 \times 10^{-5} \text{ m}^2 \text{ s}^{-1}$; hence such particles diffuse over a distance of 17 mm in about 8 s. Using $D \approx \frac{1}{3} V_c \delta$ as in Kessler (1986), this estimate was based on an average swimming distance of $\delta = 10^{-2} \text{ m}$ covered without changing direction and an average swimming speed of $V_c = 10^{-2} \text{ m s}^{-1}$ (Sloot, pers. comm.). Thus, assuming direct dependence of the growth rate on the availability of actively moving food particles and assuming that the polyps take up all the food that reaches them, the Laplacian growth assumption may be correct. In a similar way, we could estimate physical units for the growth velocities occurring in the simulations with a fixed number of advection–diffusion iterations; these results are presented elsewhere (Merks, 2003).

An interesting situation arises if we hypothesise a growth limiting resource with a lower diffusion coefficient than the ones estimated above. Examples of such slowly diffusing resources would be dissolved inorganic material, such as phosphate, nitrate or inorganic carbon (Lesser et al., 1994), whose diffusion coefficients are on the order of $10^{-9} \text{ m}^2 \text{ s}^{-1}$ (Weast et al., 2000). Assume a resource which diffuses just quickly enough to sufficiently separate the time-scales of growth and resource diffusion for a slowly growing coral. In such a case the HIRAG model would predict the growth of a widely spaced morphology and a strong degree of branch dominance. If the object would grow more quickly, according in our model the resource field would never completely stabilise, resulting in more compact and dense growth forms. Such a dependence of the morphology on the growth velocity agrees to observation and theory on diffusional growth, such as solidification. Here, a shift from a “fractal” to a “compact” morphology occurs as the growth velocities increases, thus bringing the time-scales of diffusion and growth closer together (Ihle and Müller-Krumbhaar, 1994; Brener et al., 1998). A second important condition for Laplacian growth is the model assumption that

$R = 0$ at the “coral” surface, which implies that we assume that all the resource reaching the coral surface is immediately taken up by the polyps. If we would assume instead a maximum resource uptake rate, growth would no longer be limited by the resource when resource uptake is slower than the transport of the resource to the coral. This would lead to steady resource concentrations near the coral surface, and more compact, and possibly non-branched growth forms would result.

In this paper we assumed pure diffusive transport of the resource or active random walks that we model as diffusion. At the length- and time-scales at which coral morphogenesis takes place however, convective transport and advection is likely to be of much greater importance than diffusion. If even in a glass of water convection must be put to a rest with gelatin to study pure diffusion (Vogel, 1988), it is clearly unrealistic to assume that in a dynamic environment as the ocean, besides diffusion, laminar advection and active movement, no other, faster means of resource transport would be of importance. When saturated resource uptake is assumed, such enhanced resource transport may well explain the more compact growth forms growing under the influence of water flow. We must thus be careful in interpreting our results, and realise that we have lumped together a variety of transport processes such as convection and turbulent mixing that we have modelled as advection and diffusion. The diffusion coefficients that are associated with these mixing processes and the realistic interaction of these processes with our flow obstacle—the growing coral—are the subjects of future study.

Acknowledgements

We are grateful for the very useful comments of two anonymous referees.

Appendix A. Continuous time interpretation of the accretion model

In the description of the accretive growth model, we have assumed that coral growth proceeds by the addition of layers. Indeed, in cross-sections of coral skeleton annual growth bands caused by seasonal variations in growth rates are observed (Knutson et al., 1972). However, coral polyps excrete skeleton continuously. It is more natural to model accretive growth as a time continuous process. The present model can be interpreted either as a discrete time model, in which growth proceeds by discrete time steps, or as a continuous time model, in which the accretion steps simply reflect the discretisation of a continuous process. In the latter interpretation, the displacement of a vertex

v_i can be described by

$$\frac{dz_i}{dt} = \phi_i k, \tag{A.1}$$

in which dz_i/dt is the growth velocity at vertex v_i along the local coral surface normal, and k is a constant linking resource flux to the growth velocity. After discretising Eq. (A.1)

$$z_{i,t+1} = z_{i,t} + \Delta t \frac{dz_i}{dt}(t) = z_i + \Delta t k \phi_i(t), \tag{A.2}$$

it becomes clear that parameter s [see Eq. (8)], coupling the nutrient flux to the local layer thickness, can be expressed in units of the continuous model, $s = \Delta t k$. Using the continuous time interpretation, one does not need our biological explanation to justify the normalisation of nutrient fluxes that we carry out to keep the subsequent layer thicknesses equal. In this normalisation we scale the nutrient fluxes to the maximum food flux $\phi_{max}(t)$ occurring in the simulation at time step t . The discretised form is

$$z_{i,t+1} = z_{i,t} + \Delta t k \frac{\phi_i(t)}{\phi_{max}(t)}, \tag{A.3}$$

which can be rewritten as

$$z_{i,t+1} = z_{i,t} + \Delta t^* k \phi_i(t), \tag{A.4}$$

in which $\Delta t^* = \Delta t / \phi_{max}(t)$. Hence the time step Δt^* is scaled relative to the maximum nutrient flux $\phi_{max}(t)$ and decreases as the coral colony approaches the nutrient source.

Appendix B. Mesh refinement

During an accretive growth step, the coral surface expands at convex parts of the surface, and it contracts

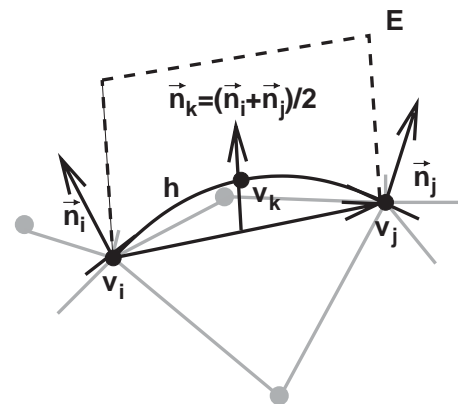


Fig. 9. Interpolation of the coral surface for vertex insertion. A third-order polynomial h is constructed, perpendicular to the surface normals \vec{n}_i and \vec{n}_j at v_i and v_j . The new vertex v_k is constructed at $v_k = (\frac{1}{2}, h(\frac{1}{2}), 0)$, relative to an orthonormal basis where $v_i = (0, 0, 0)$, $v_j = (1, 0, 0)$ and $z = 0$ at plane E . The gray lines indicate a newly constructed part of the coral surface, before vertex insertion.

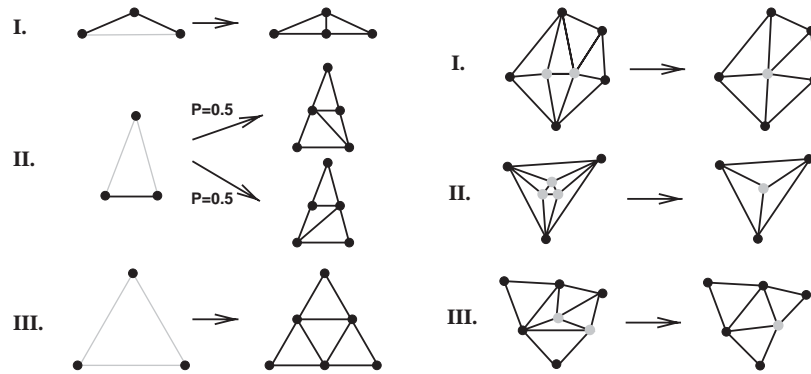


Fig. 10. Triangle insertion (left) and deletion (right) rules. Gray links are divided and gray nodes are fused. Insertion rule I: a vertex is inserted in one of the sides of the triangle. Insertion rule II: a vertex is inserted in two sides of the triangle, one of the two possible configurations is chosen at random. Insertion rule III: a vertex is inserted in all sides of the triangle. Deletion rule I: Two vertices are fused; note the expansion of the surrounding triangles. Deletion rule II: all vertices fuse. Deletion rule III: the area of the triangle is smaller than $\theta_{AREA} = 0.1 \langle A_{Tri} \rangle_{init}$, although all the edges of the triangle are larger than the fusion threshold. The triangle is removed by fusing the vertices of the shortest side.

at concave parts of the surface. In order to keep a correct and concise triangular mesh describing the coral surface, vertices are inserted and removed. Such mesh refinement is carried out according to the following rules. Two vertices fuse, if their link length $|\vec{A}_{ij}| < \theta_{FUSE}$, where θ_{FUSE} is the fusion threshold. A new, fused vertex v_k is placed at the middle of the intervertex link, and the value of $\vec{\mu}_k$ is set equal to the mean $\vec{\mu}_k = (\vec{\mu}_i + \vec{\mu}_j)/2$. Then, the vertices v_i and v_j are deleted. A new vertex is inserted between vertex v_i and v_j , if the link length $|\vec{A}_{ij}| > \theta_{INS}$. The position of the new vertex on the continuous curved surface is determined using a third-order interpolation (see Fig. 9). The insertion and fusion thresholds are set relative to the initial mean distance between the vertices $\langle |\vec{A}_{ij}| \rangle_{init}$. Insertion occurs if the distance between two vertices has grown by 50% to $\theta_{INS} = \frac{3}{2} \langle |\vec{A}_{ij}| \rangle_{init}$. The vertices fuse if their distance becomes less than half of the minimal intervertex distance directly after insertion, $\theta_{FUSE} = \frac{3}{4} \langle |\vec{A}_{ij}| \rangle_{init}$.

As vertices are inserted and deleted from the simulation, new intervertex connections are created and old ones are removed. In this way triangles are inserted and deleted from the mesh, according to the triangle insertion and deletion rules. These rules are summarised in Fig. 10.

This method of mesh refinement has a few advantages relative to the method introduced by (Kaandorp, 1994). Firstly, unlike the previously used method where subdivided triangles occurred next to undivided triangles, this refinement method generates a standard triangular mesh so that standard algorithms for triangular meshes apply. Secondly, the insertion and deletion algorithms are carried out locally to the triangles, which simplifies them relative to the previous, non-local algorithms. Thirdly, we have solved a problem in the previous mesh refinement algorithm, where always a few elongated triangles remained that were not removed by the deletion rules.

References

- Anthony, K.R.N., 1999. Coral suspension feeding on fine particulate matter. *J. Exp. Mar. Biol. Ecol.* 232, 85–106.
- Barber, C.B., Dobkin, D.P., Huhdanpaa, H., 1996. The quick-hull algorithm for convex hulls. *ACM T. Math. Software* 22, 469–483.
- Barnes, D., Chalker, B., 1990. Calcification and photosynthesis in reef-building corals and algae. In: Dubinsky, Z. (Ed.), *Coral Reefs, Ecosystems of the World*, Vol. 25. Elsevier, Amsterdam, pp. 109–131.
- Barnes, D.J., 1973. Growth in colonial scleractinians. *B. Mar. Sci.* 23, 280–298.
- Barnes, D.J., Lough, J.M., 1992. Systematic variations in the depth of skeleton occupied by coral tissue in massive colonies of *Porites* from the Great Barrier Reef. *J. Exp. Mar. Biol. Ecol.* 159, 113–128.
- Brener, E., Müller-Krumbhaar, H., Temkin, D., Abel, T., 1998. Morphology diagram of possible structures in diffusional growth. *Physica A* 249, 73–81.
- Buddemeier, R., Kinzie III, R., 1976. Coral growth. *Oceanogr. Mar. Biol. Ann. Rev.* 14, 183–225.
- Darke, W.M., Barnes, D.J., 1993. Growth trajectories of corallites and ages of polyps in massive colonies of reef-building corals of the genus *Porites*. *Mar. Biol.* 117, 321–326.
- Dauget, J.M., 1991. Application of tree architectural models to reef-coral growth forms. *Mar. Biol.* 111, 157–165.
- Gateno, D., Israel, A., Barki, Y., Rinkevich, B., 1998. Gastrovascular circulation in an octocoral: evidence of significant transport of coral and symbiont cells. *Biol. Bull.* 194, 178–186.
- Gattuso, J.P., Allemand, D., Frankignoulle, M., 1999. Photosynthesis and calcification at cellular organismal and community levels in coral reefs: a review on interactions and control by carbonate chemistry. *Am. Zool.* 39, 160–183.
- Graus, R.R., Macintyre, I.G., 1976. Light control of growth form in colonial reef corals: computer simulation. *Science* 193, 895–897.
- Graus, R.R., Macintyre, I.G., 1982. Variation in growth forms of the reef coral *Montastrea annularis* (Ellis and Solander): a quantitative evaluation of growth response to light distribution using computer simulations. *Smithson. Contrib. Mar. Sci.* 12, 441–464.
- Harriott, V.J., 1999. Coral growth in subtropical eastern Australia. *Coral Reefs* 18, 281–291.
- Huang, J., Yagel, R., Filippov, V., Kurzion, Y., 1998. An accurate method for voxelizing polygon meshes. In: 1998 ACE/IEEE Symposium on Volume Visualization. ACE/IEEE, pp. 119–126.

- Ihle, T., Müller-Krumbhaar, H., 1994. Fractal and compact growth morphologies in phase transitions with diffusion transport. *Phys. Rev. E* 49, 2972–2991.
- Kaandorp, J., 1994. *Fractal Modelling: Growth and Form in Biology*. Springer, Berlin, New York.
- Kaandorp, J.A., 1995. Analysis and synthesis of radiate accretive growth in three dimensions. *J. Theor. Biol.* 175, 39–55.
- Kaandorp, J.A., 1999. Morphological analysis of growth forms of branching marine sessile organisms along environmental gradients. *Mar. Biol.* 134, 295–306.
- Kaandorp, J.A., 2001. In: Kaandorp, J.A., Kübler, J. (Eds.), *The Algorithmic Beauty of Seaweeds, Sponges and Corals, The Virtual Laboratory*. Springer, Berlin, Heidelberg, New York, pp. 114–144.
- Kaandorp, J.A., Sloot, P.M.A., 2001. Morphological models of radiate accretive growth and the influence of hydrodynamics. *J. Theor. Biol.* 209, 257–274.
- Kaandorp, J.A., Lowe, C.P., Frenkel, D., Sloot, P.M.A., 1996. Effect of nutrient diffusion and flow on coral morphology. *Phys. Rev. Lett.* 77, 2328–2331.
- Kandhai, D., Koponen, A., Hoekstra, A.G., Kataja, M., Timonen, J., Sloot, P.M.A., 1998. Lattice-Boltzmann hydrodynamics on parallel systems. *Comput. Phys. Commun.* 111, 14–26.
- Kessler, J., 1986. Individual and collective fluid dynamics of swimming cells. *J. Fluid Mech.* 173, 191–205.
- Knutson, D.W., Buddemeier, R.W., Smith, S.V., 1972. Coral chronometers: seasonal growth bands in reef corals. *Science* 177, 270–272.
- Langdon, C., Takahashi, T., Sweeney, C., Chipman, D., Goddard, J., Marubini, F., Aceves, H., Barnett, H., Atkinson, M.J., 2000. Effect of calcium carbonate saturation state on the calcification rate of an experimental coral reef. *Glob. Biogeochem. Cycle* 14, 639–654.
- Le Tissier, M.D.A., Clayton, B., Brown, B.E., Davis, P.S., 1994. Skeletal correlates of coral density banding and an evaluation of radiography as used in sclerochronology. *Mar. Ecol.-Prog. Ser.* 110, 29–44.
- Lesser, M.P., Weis, V.M., Patterson, M.R., Jokiel, P.L., 1994. Effects of morphology and water motion on carbon delivery and productivity in the reef coral, *Pocillopora damicornis* (Linnaeus): diffusion barriers, inorganic carbon limitation, and biochemical plasticity. *J. Exp. Mar. Biol. Ecol.* 178, 153–179.
- Lough, J.M., Barnes, D.J., 1997. Several centuries of variation in skeletal extension density and calcification in massive *Porites* colonies from the great barrier reef: a proxy for seawater temperature and a background of variability against which to identify unnatural change. *J. Exp. Mar. Biol. Ecol.* 211, 29–67.
- Lough, J.M., Barnes, D.J., 2000. Environmental controls on growth of the massive coral *Porites*. *J. Exp. Mar. Biol. Ecol.* 245, 225–243.
- Loya, Y., 1976. Skeletal regeneration in a red sea scleractinian coral population. *Nature* 261, 490–491.
- Magdaleno, F.X., Casademunt, J., 1998. Surface tension and dynamics of fingering patterns. *Phys. Rev. E* 57, R3707–R3710.
- Meakin, P., 1986. A new model for biological pattern formation. *J. theor. Biol.* 118, 101–113.
- Merks, R.M.H., 2003. *Branching growth in stony corals: a modelling approach*. Ph.D. Thesis, University of Amsterdam.
- Merks, R.M.H., Hoekstra, A.G., Sloot, P.M.A., 2002. The moment propagation method for advection–diffusion in the lattice Boltzmann method: validation and Péclet number limits. *J. Comput. Phys.* 183, 563–576.
- Meyer, M., Desbrun, M., Schröder, P., Barr, A.H., 2002. Discrete differential-geometry operators for triangulated 2-manifolds. *International Workshop on Visualization and Mathematics*, Berlin-Dahlem, Germany.
- Mineev-Weinstein, M.B., Dawson, S.P., 1994. Class of nonsingular exact-solutions for Laplacian pattern formation. *Phys. Rev. E* 50, R24–R27.
- Oren, U., Rinkevich, B., Loya, Y., 1997. Oriented intra-colonial transport of C^{14} -labeled materials during coral regeneration. *Mar. Ecol.-Prog. Ser.* 161, 117–122.
- Rinkevich, B., 2001. Genetic regulation in the branching stony coral *Stylophora pistillata*. In: Kaandorp, J.A., Kübler, J.E. (Eds.), *The Algorithmic Beauty of Seaweeds, Sponges, and Corals*. Springer, Berlin, pp. 62–66.
- Rinkevich, B., 2002. The branching coral *Stylophora pistillata*: contribution of genetics in shaping colony landscape. *Isr. J. Zool.* 48, 71–82.
- Rinkevich, B., Loya, Y., 1983. Oriented translocation of energy in grafted reef corals. *Coral Reefs* 1, 243–247.
- Rinkevich, B., Loya, Y., 1985. Coral isomone: a proposed chemical signal controlling intracolony growth patterns in a branching coral. *B. Mar. Sci.* 36, 319–324.
- Sebens, K.P., Witting, J., Helmuth, B., 1997. Effects of water flow and branch spacing on particle capture by the reef coral *Madracis mirabilis* (Duchassaing and Michelotti). *J. Exp. Mar. Biol. Ecol.* 211, 1–28.
- Succi, S., 2001. *The Lattice Boltzmann Equation: For Fluid Dynamics and Beyond*. Numerical Mathematics and Scientific Computation. Oxford University Press, Oxford, New York.
- Vermeij, M.J., Barnes, D.J., Moko, S., 2001. Scleractinian stony corals (hexacorals). In: Kaandorp, J.A., Kübler, J.E. (Eds.), *The Algorithmic Beauty of Seaweeds, Sponges, and Corals*. Springer, Berlin, pp. 51–56.
- Vogel, S., 1988. *Life's Devices: The Physical World of Animals and Plants*, Chapter 8: Diffusion Versus Convection. Princeton University Press, Princeton, NJ, pp. 158–176.
- Weast, R.C., Astle, M.J., Beyer, W.H. (Eds.), 2000. *CRC Handbook of Chemistry and Physics*, 3rd Electronic Edition. CRC Press, Boca Raton, FL.
- Wells, J.W., 1969. The formation of dissepiments in zooantharian corals. In: Campbell, K.S.W. (Ed.), *Stratigraphy and Paleontology*. Australian National University Press, Canberra, pp. 17–26.
- Witten Jr., T., Sander, L., 1981. Diffusion-limited aggregation, a kinetic critical phenomenon. *Phys. Rev. Lett.* 47, 1400–1403.